Estimating total magnetization direction using equivalent-layer technique

(August 22, 2019)

Running head: **Determining total magnetization direction**

ABSTRACT

We developed a new method for estimating the total magnetization direction of magnetic sources based on equivalent-layer technique using total-field anomaly data. This approach does not impose strong information either about the shape or about the depth of the sources, and does not require a regularly spaced data. Usually, this equivalent-layer technique is used for processing total-field anomaly data by estimating a 2D magnetic-moment distribution over a fictitional layer composed by dipoles below the observation plane. When the magnetization direction of equivalent sources is almost the same as the true body, the estimated magnetic property over the layer is all positive. Iteratively, the proposed method imposes zeroth-order Tikhonov regularization and positivity constraint on the estimated magnetic moment over the layer and estimate the magnetization direction of the geological sources. Mathematically, the algorithm solves least-squares problems in two steps: the first one solves a linear inverse problem for estimating a 2D magnetic-moment distribution within the equivalent layer and the second solves a nonlinear inverse problem for magnetization direction of the magnetized sources. We test the methodology by applying to synthetic data for complicated geological scenarios, and the results show that the method can be a powerful tool for estimating the magnetization direction of a set of bodies. Tests on field data from Goias Alkaline Province (GAP), center of Brazil, over Montes Claros complex

suggests intrusions with remarkable strong remanent magnetization, in agreement with the current literature for this region.

INTRODUCTION

The magnetic method is one of the oldest geophysical technique that plays an important role in exploration geophysics. This method has been applied for interpreting a vast geological scenarios like estimating the basement relief, mapping faults and lithological contacts, defining bounds of geological sources, determining the position of salt domes whithin sediments, and indentifying oil and gas traps. With the improvement of magnetic measurements, mainly by the use of aeromagnetic surveys providing a large amount of data, this technique has become standard in geophysics to map areas with a variety of scales (Blakely, 1996; Nabighian et al., 2005). In order to better describe the subsurface structures, it is necessary to extract a reliable information from magnetic data.

The magnetization direction is very important to interpret magnetic anomalies allowing to characterize the exploration targets. Hence, several techniques for estimating magnetization direction have been emerged through the last years. The strategies for estimating this quantity can be divided into two main groups. The first one comprises the methods which presume a priori information about the shape of geological sources. Bhattacharyya (1966) presented an iterative method for determining the parameters of a rectangular prismatic shape, such as horizontal dimensions, depth of the body and magnetization direction. Emilia and Massey (1974) approximate the a seamount by a set of stacked prism with the same magnetization direction and different magnetization intensity. Parker et al. (1987) proposed a method for estimating de magnetization direction formulating as an optimization problem by imposing an uniformly magnetization distribution. Ryuji and Uchiyama (2005) also parametrized a seamoumt approximating by a set of juxtaposed prisms and estimating the magnetization direction of each one. Finally, Oliveira Jr et al. (2015) approximate a

magnetic source by a spherical geometry, assumig the knowledge of the center and estimating the magnetization direction. The second group are the methods which not presume any information about the magnetic source. Fedi et al. (1994), for example, proposed a method that performs a succesive reduction-to-pole on frequency domain testing it for a set of magnetization direction. Medeiros and Silva (1995) presented an interpretation method that estimates the total magnetization direction and the spatial orientation of the source based on the multipole expansion. Phillips (2005) implemented an algorithm that uses the Helbig's integral for estimating the three-component vector of the magnetic-dipole moment. Tontini and Pedersen (2008) extended the method using the same Helbig's integral to estimate the magnetization direction and its magnitude, also providing information about the position of the centre of magnetization distribution. Lelivre and Oldenburg (2009) developed a method for estimating the magnetization direction in complex geological scenarios. In addition, there are the methods that are based on the correlation of potential quantities (Dannemiller and Li, 2006; Gerovska et al., 2009; Liu et al., 2015; Zhang et al., 2018).

Estimating the magnetization direction is extremely important not only for interpretation, but also for processing the total-field anomaly data. One technique in spatial domain commonly used for processing potential-field data is the equivalent layer. It was first introduced by Dampney (1969) and Emilia and Massey (1974) for processing gravity and magnetic data, respectively. After these pioneer works, this technique has been widely used for processing such as interpolation (Cordell, 1992; Mendonça and Silva, 1994; Barnes and Lumley, 2011; Siqueira et al., 2017), upward (or downward) continuation (Hansen and Miyazaki, 1984; Li and Oldenburg, 2010), reduction to the pole (Silva, 1986; Leão and Silva, 1989; Guspí and Novara, 2009; Oliveira Jr. et al., 2013), computing the amplitude of anomalous field (Li and Li, 2014) and denoising gradient data (Martinez and Li, 2016).

The equivalent layer approach consists to approximate the observed and predicted data produced by a set of discrete sources (e.g., prisms, dipoles or point masses) commonly known as equivalent sources. Once the physical property in the layer is estimated, it can be used for processing potential-field data. Nevertheless, prominent discussions about the physical-property estimated over the layer are increasing in the last decades. For example, Pedersen (1991) discussed the relation between potential field and equivalent source. Weiss et al. (2007), using magnetic microscopy data, pointed out that fixing a magnetization direction the magnetic-moment estimated in the layer are all-positive. Baratchart et al. (2013) show that, assuming the unidirectional solution, its possible to achieve uniqueness on the inverse problem. Lima et al. (2013) proposed a method on the frequency domain to investigate the unidirectional solution on a planar geological sample with magnetic microscopy data, showing that the physical-property estimated over the layer is entirely positive. On the other hand, Li et al. (2014a) using total-field anomaly data, proved the existence of a positive distribution over the layer, and its a sufficient feature to overcome the low-latitude instability. However, these authors considered only a purely induced magnetization for the magnetic sources.

We present a new method using total-field anomaly data that estimates the magnetization direction without presume any information about the magnetic sources. It is based on the exploration of the theoretical aspect of positivity to build a nested algorithm to solve the inverse problem. We examine the performance of the method testing it in synthetic tests generated by complex geological scenarios. Furthermore, application to field data from Gois alkaline province (GAP) over the Montes Claros complex, center of Brazil, shows the performance of the method in estimating a meaningful magnetization direction. The result suggests the presence of a remarkable remanent magnetization.

METHODOLOGY

Fundamentals of magnetic equivalent layer and the positive magnetic-moment distribution

Considering a Cartesian coordinate system with x-, y- and z-axis being oriented to north, east and downward, respectively. Let $\Delta T_i \equiv \Delta T(x_i, y_i, z_i)$ be the total-field anomaly, at the ith position (x_i, y_i, z_i), produced by a continuos layer located below the observation plane at a depth equal to z_c, where $z_c > z_i$, and $p(x', y', z_c)$ is the distribution of magnetic dipoles moment per unit area over the layer. The total-field anomaly produced by this continuous layer is given by

$$\Delta T_i = \int_{-\infty}^{+\infty}\int_{-\infty}^{+\infty} p(x', y', z_c)[\gamma_m \hat{\mathbf{F}}_0^T \mathbf{M}(x_i, y_i, z_i, x', y', z_c)\, \hat{\mathbf{m}}(\mathbf{q})]dx'\, dy', \tag{1}$$

where γ_m is a constant proportional to the vacuum permeability, $\hat{\mathbf{F}}_0$ is a unit vector with the same direction of the main geomagnetic field given by

$$\hat{\mathbf{F}}_0 = \begin{bmatrix} \cos I \cos D \\ \cos I \sin D \\ \sin I \end{bmatrix}, \tag{2}$$

where I and D are, respectively, the inclination and declination and $\mathbf{M}(x_i, y_i, z_i, x', y', z_c)$ is a 3×3 dimensional matrix (Oliveira Jr et al., 2015) equal to

$$\mathbf{M}(x_i, y_i, z_i, x', y', z_c) = \begin{bmatrix} \partial_{xx}\phi & \partial_{xy}\phi & \partial_{xz}\phi \\ \partial_{yx}\phi & \partial_{yy}\phi & \partial_{yz}\phi \\ \partial_{zx}\phi & \partial_{zy}\phi & \partial_{zz}\phi \end{bmatrix}, \tag{3}$$

where $\partial_{\alpha\beta}\phi$, $\alpha = x, y, z$ and $\beta = x, y, z$, is the second derivative of the scalar function

$$\phi(x_i, y_i, z_i, x', y', z_c) = \frac{1}{[(x_i - x')^2 + (y_i - y')^2 + (z_i - z_c)^2]^{\frac{1}{2}}}. \tag{4}$$

with respect to the Cartesian coordinates x_i, y_i and z_i of the observation points. The $\hat{\mathbf{m}}(\mathbf{q})$ is a unit vector with the magnetization direction of the dipoles over layer given by

$$\hat{\mathbf{m}}(\mathbf{q}) = \begin{bmatrix} \cos\tilde{\imath}\cos\tilde{d} \\ \cos\tilde{\imath}\sin\tilde{d} \\ \sin\tilde{\imath} \end{bmatrix} \tag{5}$$

and $\mathbf{q}$ is a 2×1 vector with components given by

$$\mathbf{q} = \begin{bmatrix} \tilde{\imath} \\ \tilde{d} \end{bmatrix}, \tag{6}$$

where $\tilde{\imath}$ and $\tilde{d}$ are the inclination and declination of the magnetization direction of the dipoles on the layer, respectively. We can also notice that the vector defined in equation 5 has a single and uniform magnetization direction of all dipoles on the layer. For convenience, this unit vector can be rewritten as follows

$$\hat{\mathbf{m}}(\mathbf{q}) = \mathbf{R}\hat{\mathbf{h}}\,, \tag{7}$$

where $\hat{\mathbf{h}}$ defines the uniform magnetization direction of an abitrary magnetic source and $\mathbf{R}$ is a 3×3 matrix obtained from Euler's rotation theorem. This theorem states that any rotation can be parametrized by using three parameters called Euler angles (H. Goldstein and Safko, 1980). That is, if all dipoles that set up the equivalent layer have the same magnetization direction $\hat{\mathbf{m}}(\mathbf{q})$ and this direction is the same as the true magnetic source $\hat{\mathbf{h}}$,

then the matrix $\mathbf{R}$ (equation 7) is equal to identity. For this reason, the total-field anomaly produced by equivalent layer at the ith position (x_i, y_i, z_i) (equation 1) can be rewritten as

$$\Delta T_i = \int_{-\infty}^{+\infty}\int_{-\infty}^{+\infty} p(x', y', z_c)[\gamma_m \hat{\mathbf{F}}_0^T \mathbf{M}(x_i, y_i, z_i, x', y', z_c)\,\hat{\mathbf{h}}]dx'\,dy', \tag{8}$$

which represents the total-field anomaly produced by continuous layer with the same direction of the arbitrary magnetic source. Thus, the reduction to the pole (RTP) field ΔT_i^{PL} produced by equivalent layer at the point (x_i, y_i, z_i) is equal to

$$\Delta T_i^{PL} = \int_{-\infty}^{+\infty}\int_{-\infty}^{+\infty} p(x', y', z_c)[\gamma_m \partial_{zz}\phi(x_i, y_i, z_i, x', y', z_c)]dx'\,dy', \tag{9}$$

where $\partial_{zz}\phi(x_i, y_i, z_i, x', y', z_c)$ is the second derivative of the inverse of distance (equation 4) with respect of z_i, evaluated at the point (x_i, y_i, z_i). However, by considering the RTP field ΔT_i^{PS} that would be produced by an arbitrary uniformly magnetized source at the pole, we have

$$\Delta T_i^{PS} = \gamma_m \partial_{zz}\Gamma(x_i, y_i, z_i)\, m, \tag{10}$$

where m is the magnetization intensity of the magnetic source. The $\partial_{zz}\Gamma(x_i, y_i, z_i)$ is the second derivative in relation to z_i of a scalar function $\Gamma(x_i, y_i, z_i)$

$$\Gamma(x_i, y_i, z_i) = \iiint_{\upsilon} \frac{d\upsilon}{[(x_i-\alpha)^2 + (y_i-\beta)^2 + (z_i-\gamma)^2]^{\frac{1}{2}}} \tag{11}$$

in which α, β and γ are the Cartesian coordinates of an infinitesimal element inside the volume υ of the magnetic source. From equation 9 and 10, we obtain

$$m\,\partial_{zz}\Gamma(x_i, y_i, z_i) = \int_{-\infty}^{+\infty}\int_{-\infty}^{+\infty} p(x', y', z_c)\partial_{zz}\phi(x_i, y_i, z_i, x', y', z_c)dx'\,dy'. \tag{12}$$

We can notice that equation 12 can be calculated differentiating the following equation

$$m\,\partial_{z}\Gamma(x_i, y_i, z_i) = \int_{-\infty}^{+\infty}\int_{-\infty}^{+\infty} \frac{p(x', y', z_c)(z_c - z_i)}{[(x_i - x')^2 + (y_i - y')^2 + (z_i - z_c)^2]^{\frac{3}{2}}}dx'\,dy' \tag{13}$$

with respect to the vertical component z_i, where $z_c > z_i$.

From potential-field theory, we can highlight the classical upward continuation integral

$$U(x_i, y_i, z_i) = \frac{(z_c - z_i)}{2\pi}\int_{-\infty}^{+\infty}\int_{-\infty}^{+\infty} \frac{U(x', y', z_c)}{[(x_i - x')^2 + (y_i - y')^2 + (z_i - z_c)^2]^{\frac{3}{2}}}dx'\,dy', \tag{14}$$

where the function $U(x_i, y_i, z_i)$ is an hamornic function at all (x_i, y_i, z_i) and $U(x', y', z_c)$ is the same harmonic function at (x', y', z_c) (Blakely, 1996). In this case, if this harmonic function represents the total-field anomaly at the point (x_i, y_i, z_i), it can be mathematically interpreted as the convolution between its values $U(x', y', z_c)$ and the vertical derivative with respect to z_i of the equation 4, evaluated on the horizontal plane $z_i = z_c$. Therefore, according to the classical upward continuation function (equation 14), the magnetic-moment distribution $p(x', y', z_c)$ in equation 13 assumes the form

$$p(x', y', z_c) = \frac{m}{2\pi}\,\partial_z\Gamma(x', y', z_c), \tag{15}$$

where $\partial_z\Gamma(x', y', z_c)$ is the derivative of the scalar function 11 in relation to z_i evaluated over the equivalent layer. The most interesting aspect of equation 15 is that the magnetic-moment distribution is defined as the product of a positive constant $\frac{m}{2\pi}$ and the function $\partial_z\Gamma(x', y', z_c)$, which is all positive at all points (x', y', z_c) over the equivalent layer. This

relation is similar to that presented by Pedersen (1991) and Li et al. (2014b). In the wavenumber domain, these authors determined the magnetic-moment distribution within a continuous equivalent layer with the same magnetization direction as the local-geomagnetic field at the pole. They also considered a planar equivalent layer located below and parallel to a horizontal plane containing the observed total-field anomaly. They assume a magnetic source having a purely induced magnetization. Under these assumptions, Pedersen (1991) and Li et al. (2014b) concluded that the magnetic-moment distribution within the continuous equivalent layer is proportional to the pseudogravity anomaly produced by the source on the plane of the equivalent layer. By following different approaches using magnetic microscopy data, Baratchart et al. (2013) and Lima and Weiss (2016) pointed out by imposing a nonnegativity constraint, the solution to the inverse problem is a unique magnetic-moment distribution. Here, we do not follow the same wavenumber-domain reasoning used by all these authors. Moreover, equation 15 generalizes this positivity condition because (1) it holds true for all cases in which the magnetization of the equivalent layer has the same direction as the true magnetization of the sources, whether it is purely induced or not, (2) does not require that the observed total-field anomaly data be on a plane and, (3) does not require a planar equivalent layer.

Parametrization and forward problem

In practical situations, it is not possible to determine a continuous magnetic-moment distribution $p(x', y', z_c)$ over the layer as shown in equation 1. For this reason, the layer has to be approximated by a discrete set of dipoles with unit volume located at a constant depth $z = z_c$. By discretizing the integrand of equation 1, the predicted total-field anomaly at the point (x_i, y_i, z_i) is given by

$$\Delta T_i = f_i(\mathbf{s}), \tag{16}$$

where ΔT_i is the ith element of the N-dimensional vector of predicted total-field anomaly $\mathbf{\Delta T}(\mathbf{s})$. The function f_i maps the unknown parameters onto the data, in which the parameter vector $\mathbf{s}$ is formed by an M-dimensional vector $\mathbf{p}$ whose jth element p_j is the magnetic moment of the jth dipole with a single magnetization direction $\mathbf{q}$ (equation 6) assigned to all dipoles (Figure 1). Explicitly, the function f_i is described as

$$f_i(\mathbf{s}) = \sum_{j=1}^{M} p_j g_{ij}(\mathbf{q}), \tag{17}$$

where

$$g_{ij}(\mathbf{q}) = \gamma_m \hat{\mathbf{F}}_0^T \mathbf{M}_{ij} \hat{\mathbf{m}}(\mathbf{q}) \tag{18}$$

is an harmonic function representing the total-field anomaly at the ith position (x_i, y_i, z_i) yielded by a jth dipole located at (x_j, y_j, z_c) with unit magnetic-moment intensity. The matrix $\mathbf{M}_{ij}$ is formed by the second derivatives of a function ϕ_{ij} that depends on the inverse of the scalar function $r_{ij} = [(x_i - x_j)^2 + (y_i - y_j)^2 + (z_i - z_c)^2]^{1/2}$, analogously to equations 3 and 4. From equations 16-18, we can notice that the predicted total-field anomaly $\mathbf{\Delta T}(\mathbf{s})$ has a linear relation with the magnetic moment $\mathbf{p}$ and a nonlinear relation with the magnetizaion direction $\mathbf{q}$.

Inverse problem

Let $\mathbf{\Delta T}^o$ be an N-dimensional vector whose ith element ΔT_i^o is the total-field anomaly observation produced by a magnetic source at the point (x_i, y_i, z_i), $i = 1, \ldots, N$. In order to

estimate the magnetization direction, we have to formulate an inverse problem by imposing a positivity constraint on the magnetic-moment distribution. Here, it is accomplished by solving the following constrained problem of

$$\text{minimizing} \qquad \Psi(\mathbf{s}) = \|\boldsymbol{\Delta}\mathbf{T}^o - \boldsymbol{\Delta}\mathbf{T}(\mathbf{s})\|_2^2 + \mu f_0 \parallel \mathbf{p} \parallel_2^2 \tag{19a}$$

$$\text{subject to} \qquad \mathbf{p} \geqslant 0. \tag{19b}$$

On the right side of equation 19a the first and second terms are the data-misfit function and the zeroth-order Tikhonov regularization function, μ is the regularizing parameter, $\|\cdot\|_2^2$ represents the squared Euclidean norm and f_0 is a normalizing factor. In the inequality 19b, $\mathbf{0}$ is a null vector and the inequality sign is applied element by element. This inequality imposes positivity constraints on the estimated magnetic moments of all dipoles, which is solved by using the nonnegative least squares (NNLS) proposed by Lawson and Hanson (1974).

Minimizing the goal function shown in equation 19a starts with an initial approximation $\mathbf{s}^k$ to the parameter vector and then solving a sequence of linear problem of estimating a correction $\boldsymbol{\Delta}\mathbf{s}^k$ at each kth iteration. The procedure is repeated until a minimum of goal function (equation 19a) is reached. This procedure is determined by using a gradient-based iterative optimization method like Gauss-Newton (Aster et al., 2005). Mathematically, the correction $\boldsymbol{\Delta}\mathbf{s}^k$ is expressed as a second-order expansion of the goal function given by

$$\Psi(\mathbf{s}^k + \boldsymbol{\Delta}\mathbf{s}^k) \approx \Psi(\mathbf{s}^k) + \mathbf{J}^{k^T}(\mathbf{s}^k)\boldsymbol{\Delta}\mathbf{s}^k + \frac{1}{2}\boldsymbol{\Delta}\mathbf{s}^{k^T}\mathbf{H}^k(\mathbf{s}^k)\boldsymbol{\Delta}\mathbf{s}^k \tag{20}$$

in which $\mathbf{J}^k(\mathbf{s}^k)$ and $\mathbf{H}^k(\mathbf{s}^k)$ are, respectively, the gradient vector and the Hessian matrix of equation 19a. Thus, taking the gradient with respect to the parameter perturbation

vector $\mathbf{\Delta s}^k$ of the expanded equation 20 and setting the result equal to the null vector, it is obtained by solving the linear system

$$\mathbf{H}^k(\mathbf{s}^k)\mathbf{\Delta s}^{\sharp^k} = -\mathbf{J}^k(\mathbf{s}^k), \tag{21}$$

where the estimate $\mathbf{\Delta s}^{\sharp^k}$ is a single step of the Gauss-Newton method required to attain the minimum of the expanded function (equation 20). The linear system given by equation 21 can be rewritten as

$$\left[\begin{array}{c|c} \mathbf{H}_{pp}^k & \mathbf{H}_{pq}^k \\ \hline \mathbf{H}_{qp}^k & \mathbf{H}_{qq}^k \end{array}\right] \left[\begin{array}{c} \mathbf{\Delta p}^k \\ \\ \mathbf{\Delta q}^k \end{array}\right] = - \left[\begin{array}{c} \mathbf{J}_p^k \\ \\ \mathbf{J}_q^k \end{array}\right], \tag{22}$$

in which $\mathbf{J}_\alpha^k$ and $\mathbf{H}_{\alpha\beta}^k$, where $\alpha = p, q$ and $\beta = p, q$, are the gradient vector and the Hessian matrix calculated in relation to each element of the magnetic-moment vector $\mathbf{p}$ and the magnetization direction vector $\mathbf{q}$, respectively. Besides, in order to simplify the equation 22, we consider null cross-derivatives.

However, The gradient vector and the Hessian matrix relative to the part of magnetic moments are, respectively,

$$\mathbf{J}_p^k = -2\mathbf{G}_p^{k^T}[\mathbf{\Delta T}^o - \mathbf{\Delta T}(\mathbf{s}^k)] + 2\mu f_0^k \mathbf{p}^k \tag{23}$$

and

$$\mathbf{H}_{pp}^k = 2\mathbf{G}_p^{k^T}\mathbf{G}_p^k + 2\mu f_0^k \mathbf{I} \tag{24}$$

where $\mathbf{G}_p^k$ is the $N \times M$ sensitivity matrix at the kth iteration, whose ijth element is given by equation 18, $\mathbf{I}$ is an identity matrix and the normalizing factor f_0^k is equal to

$$f_0^k = \frac{tr(\mathbf{G}_p^{k^T}\mathbf{G}_p^k)}{M}\,, \tag{25}$$

where tr is denotaded as the trace of the matrix $\mathbf{G}_p^{k^T}\mathbf{G}_p^k$ and M is the total number of dipoles composing the layer. From the correction $\boldsymbol{\Delta}\mathbf{p}^{\sharp^k} = \mathbf{p}^{\sharp^{k+1}} - \mathbf{p}^{\sharp^k}$, we can conclude that the linear system to be solved is given by

$$\left[\mathbf{G}_p^{k^T}\mathbf{G}_p^k + \mu f_0^k\mathbf{I}\right]\mathbf{p}^{\sharp^{k+1}} = \mathbf{G}_p^{k^T}\boldsymbol{\Delta}\mathbf{T}^o. \tag{26}$$

Owing to nonlinear relation of the magnetization direction $\mathbf{q}^k$ with the predicted total-field anomaly, the gradient vector and the Hessian matrix at the kth for this case are, respectively,

$$\mathbf{J}_q^k = -2\mathbf{G}_q^{k^T}[\boldsymbol{\Delta}\mathbf{T}^o - \boldsymbol{\Delta}\mathbf{T}(\mathbf{s}^k)] \tag{27}$$

and

$$\mathbf{H}_{qq}^k = 2\mathbf{G}_q^{k^T}\mathbf{G}_q^k \tag{28}$$

in which $\mathbf{G}_q^k$ is a $N \times 2$ sensitivity matrix, whose elements are composed by derivative of equation 17 in relation of each element of the vector $\mathbf{q}^k$, that are the inclination and declination. Nevertheless, to calculate the correction $\boldsymbol{\Delta}\mathbf{q}^{\sharp^k}$ at the kth iteration, we use the Levernberg-Marquardt method (Aster et al., 2005) by solving the linear system

$$\left[\mathbf{G}_q^{k^T}\mathbf{G}_q^k + \lambda^k\mathbf{I}\right]\boldsymbol{\Delta}\mathbf{q}^{\sharp^k} = \mathbf{G}_q^{k^T}[\boldsymbol{\Delta}\mathbf{T}^o - \boldsymbol{\Delta}\mathbf{T}(\mathbf{s}^k)], \tag{29}$$

where λ is the Marquardt parameter that is updated along the iterative process and $\mathbf{I}$ is an indentity matrix. After estimating the parameter correction $\boldsymbol{\Delta}\mathbf{q}^{\sharp^k}$ at the kth iteration, we

update the magnetization direction such that

$$\mathbf{q}^{\sharp k+1} = \mathbf{q}^{\sharp k} + \boldsymbol{\Delta}\mathbf{q}^{\sharp k}. \tag{30}$$

Iterative process for magnetization estimation

The magnetic moments $\mathbf{p}^{\sharp}$ and the magnetization direction $\mathbf{q}^{\sharp}$ are obtained through an inverse problem of minimizing the difference between the observed data $\boldsymbol{\Delta}\mathbf{T}^{o}$ and the predicted data $\boldsymbol{\Delta}\mathbf{T}(\mathbf{s})$. As we can notice, the solution of the inversion is given by solving two linear systems shown in equation 26 and equation 29. For this reason, we propose a nested algorithm for solving the inverse problem in two steps.

Our iterative algorithm starts with an initial guess for the magnetization direction $\mathbf{q}_0$. At the kth iteration, we estimate a set of magnetic moment $\mathbf{p}^{\sharp k+1}$ by imposing a positivity constraint on equation 26. After estimating the magnetic-moment distribution $\mathbf{p}^{\sharp k+1}$ within the equivalent layer at the kth iteration using the previous estimate $\mathbf{q}^{\sharp k}$ for the magnetization direction, we estimate the corrections of magnetization direction vector $\boldsymbol{\Delta}\mathbf{q}^{\sharp k}$ by solving the unconstrained nonlinear inverse problem (equation 29) and update the magnetization direction by equation 30. The iterative process stops when the goal function (equation 19a) is invariant along successive iterations. An overview of the algorithm is shown in Figure 2 and in the algorithm 1.

Algorithm 1: Nested NNLS and Levenberg-Marquardt method

Input : $\mathbf{\Delta T}^o$, $\mathbf{q}_0$

Output: $\mathbf{p}^\sharp$,$\mathbf{q}^\sharp$

while *(not converge) or* $(i < i_{max})$ **do**

  step 1: Solve equation 26 using NNLS ;

  step 2: Compute goal function (equation 19a) ;

  while *(not converge) or* $(j < j_{max})$ **do**

    step 3: Initialize the Levenberg-Marquardt algorithm ;

    step 4: Compute goal function (equation 19a);

    while $k < k_{marq}$ **do**

      step 5: Solve equation 29 ;

      step 6: Update the magnetization direction estimate (equation 30) ;

      step 7: Compute goal function (equation 19);

    end

    step 8: Analysis of convergence for inner loop.

  end

  step 9: Analysis of convergence for outer loop.

end

The choice of layer depth $\mathbf{z_c}$ and regularization parameter μ

The procedure for the use of our methodology for estimating the total magnetization require the choice of two main parameters. The first one is the layer depth z_c as shown in Figure 1 and the second is the regularization parameter μ shown in equation 26.

The method of the choice of layer is based on a classical approach proposed by Dampney

(1969). The author pointed out that the layer depth should satisfy an interval from 2.5 to 6 times the grid spacing. It should be notice that this rule was applied on an evenly spaced data. However, the choice for applying our method should correspond to an interval from 2 to 3 times the greater grid spacing. It is necessarily to point out that this range of values was found empirically due to the application on a irregular grid data.

To solve the equation 26 we have to choose a reliable regularization parameter μ. For this purpose, we use the L-curve method (Hansen and OLeary, 1993). This approach is widely used in the literature to find a regularizing parameter, which filtering out enough noise without loosing to much information in the final solution. The procedure of finding the parameter plot a curve of optimal values between the solution norm and residual norm. The corner of the curve is the optimal regularization parameter which gives a threshold between the regularizing function and the data misfit.

APPLICATION TO SYNTHETIC DATA

We applied the proposed method to three synthetic data sets simulating different geological scenarios. The first one is generated by a model containing a set of multiple sources with different geometries, all of them with the same magnetization direction. The second data set is generated by a set of multiple magnetic bodies, but one them being a shallow-seated source with the same magnetization direction. In the third test, we violate the hypothesis of unidirectional magnetization by simulating a shallow-seated source with different magnetization direction from the other bodies.

In all tests, the simulated data were computed on a regular grid of 49×25 points (with a total of $N = 1225$ observations) at a constant height of 100 m. We assume an observation area extending 12 km along the x- and y-axis, resulting a grid spacing of 250 m and 500 m on x- and y-axes, respectively. The data were contamined with pseudorandom Gaussian noise with zero mean and 10 nT standard deviation. The geomagnetic field direction simulated was $I = -40^\circ$ and $D = -22^\circ$ for the inclination and declination, respectively. In the inversion, we use an equivalent layer composed by a grid of 49×25 dipoles (with a total of $M = 1225$ equivalent sources) positioned at a depth of $z_c = 1150$ m below the observation plane (2.5 times the greater grid spacing). We use the L-curve to choose the regularizing parameter (μ). Our algorithm starts with an initial guess $\mathbf{q}_0 = (-10^\circ, -10^\circ)$ for inclination and declination, respectively.

Unidirectional magnetization sources

We generate a 3D prism with polygonal cross-section whose the top is positioned at a depth of 450 m and the bottom 3150 m with magnetization intensity of 4 A/m. We also generate

two spheres with magnetization intensity equal to 3 A/m and radius equal to 500 m. The coordinates of the spheres centers $x_c = 1800$ m, $y_c = -1800$ m and $z_c = 1000$ m and $x_c = 800$ m, $y_c = 800$ m and $z_c = 1000$ m. We produce two rectangular prisms with 2.5 A/m of magnetization intensity. The smaller prism has the top at a depth of 450 m and side lengths of 1000 m, 700 m and 500 m along x-,y- and z-axes, respectively. The greater prism has the top at a depth of 500 m and side lengths of 1000 m, 2000 m and 1550 m along x-,y- and z-axes. All simulated sources have inclination $-25°$ and declination $30°$. The noise-corrupted data is shown in Figure 3a.

Figure 3b shows the predicted data produced by equivalent layer. Figure 3c shows the residuals defined as the difference between the simulated data (Figure 3a) and the predicted data (Figure 3b). The residuals appear normally distributed with a mean of $-0.30\,nT$ and a standard deviation of $9.67\,nT$ as shown in Figure 3d. The estimated magnetization direction $\mathbf{q}^\sharp$ has inclination $-28.6°$ and declination $30.8°$ which are very close to the true one. Figure 3e shows the estimated magnetic-moment distribution $\mathbf{p}^\sharp$. The convergence of the algorithm is shown in Figure 3f. These results show that the all-positive magnetic-moment distribution and the estimated magnetization direction produce an acceptable data fitting.

Unidirectional magnetization with shallow-seated source

Here, we test the methodology perfomance when a shallow-seated source exists. The model seems the previous test except for the smaller prism, whose the top is 150 m deep while maintaining its volume. The magnetization intensity of this shallow prism is equal to 1.5 A/m. The magnetization direction of all sources is $-25°$ inclination and declination $30°$, respectively. The synthetic data is shown in Figure 4a.

Figure 4b shows the predicted total-field anomaly produced by equivalent layer. Figure 4c shows the residuals defined as the difference between the simulated data (Figure 4a) and the predicted data (Figure 4b). The residuals appear normally distributed with a mean of -0.42 nT and a standard deviation of 10.67 nT as shown in Figure 4d. Figure 4e shows the estimated magnetic-moment distribution $\mathbf{p}^\sharp$. The convergence of the algorithm is shown in Figure 4f. Despite the large residual located above the shallow-seated source, we consider that the methodology produced a reliable result because the estimated magnetization direction $\mathbf{q}^\sharp$ has inclination -28.7° and declination 31.7° and its very close to the corresponding true magnetization direction, and the all-positive magnetic-moment distribution produces an acceptable data fitting.

Shallow-seated source with different magnetization direction

In this test, we simulate the presence of a shallow-seated body with different magnetization direction from the other magnetic sources. The shallow prism has the dimension and magnetization intensity equal to the previous test. However, the magnetization direction of the shallow prism is 20° of inclination and -30° of declination, while the other sources has inclination -25° and declination 30°. The noise-corrupted data is shown in Figure 5a.

Figure 5b shows the predicted total-field anomaly. Figure 5c shows the residuals defined as the difference between the simulated data (Figure 5a) and the predicted data (Figure 5b). The residuals have a mean of -0.71 nT and a standard deviation of 10.67 nT as shown in Figure 5d. The estimated magnetization direction $\mathbf{q}^\sharp$ has inclination -30.4° and declination 27.6°. Figure 5e shows the estimated magnetic-moment distribution $\mathbf{p}^\sharp$. The convergence of the algorithm is shown in Figure 5f. Despite the slight difference from

the true magnetization direction, the estimated magnetic-moment distribution produces an acceptable data fit. With the exception of the small area exactly above the small-seated prism most of the residuals are closely 0 nT.

APPLICATION TO FIELD DATA

The Goias alkaline province (GAP) is a region in the central part of Brazil that there are occurences of mafic-ultramafic alkaline magmatism. This region presents a variety of rocks with an extense petrographic types. Throughout the area there are mafic-ultramafic complexes (plutonic intrusions), subvolcaninc alkaline intrusions (diatremes) and volcanic products (kamafugite lava flows) with several dikes. Some of the main alkaline complexes of GAP are: the Montes Claros de Goiás, Diorama, Corrego dos Bois, Morro do Macaco and Fazenda Buriti. These alkaline intrusions are sorrounded by a Precambrian basement and the Phanerozoic sedimentary rocks of the Paraná Basin. (Junqueira-Brod et al., 2005; Carlson et al., 2007; Marangoni and Mantovani, 2013; Dutra et al., 2014). Recent studies indicate the existence of a remarkable remanent magnetization component within these intrusions (Marangoni and Mantovani, 2013; Oliveira Jr et al., 2015; Marangoni et al., 2016; Zhang et al., 2018).

The aeromagnetic survey has a flight pattern with north-south spaced from $\sim$ 500 m and $\sim$ 8 m along each line, and a constant height of 100 m from the terrain. The geomagnetic field direction for this area was $-19.5°$ and $-18.5°$ for inclination and declination, respectively. We invert the total-field anomaly (Figure 6a) from the alkaline complex of Montes Claros. To speed up data processing and inversion, we downsampled the data along the flight lines, resulting a grid of 55×32 points (a total of $N = 1787$ observations). This new set up results an approximately 320 m and 470 m grid spacing along the x- and y-axes, respectively. We use an equivalent layer composed by a grid of 55×32 dipoles (a total of $M = 1787$ equivalent sources) positioned at a depth of 840 m below the observation plane ($\sim$ 2 times the greater grid spacing). The algorithm starts with an initial guess of $-70°$

and 50° for the inclination and declination, respectively. Figure 6b shows the predicted data produced by equivalent layer. Figure 6c shows the residuals defined as the difference between the observed data (Figure 6a) and the predicted data (Figure 6b). Notice that, two small places in Figure 6d where large residuals are clearly apparent may indicate the existence of shallow-seated geologic sources with different magnetization direction. However, the histogram of residuals (Figure 6d) is acceptable with its mean of -14.52 nT ($\sim 0.1\%$ of the maximum value of total-field anomaly data) and standard deviation of 312.28 nT ($\sim 2\%$ of the maximum value of total-field anomaly data). The estimated magnetization direction $\mathbf{q}^\sharp$ has inclination $-50.2°$ and declination 34.9°. Figure 6e and 6f shows the estimated magnetic-moment distribution $\mathbf{p}^\sharp$ and the convergence of the algorithm. We check the quality of the estimated magnetization direction by computing the reduction-to-pole of the observed total-field anomaly. We can notice that the RTP field anomaly (Figure 7) exhibits predominantly positive values and decays to zero towards the borders of study area. For this reason, we consider that the estimated magnetization direction led to a satisfactory RTP anomaly. We conclude with these results that the all-positive magnetic moment distribution and the estimated magnetization direction produce an acceptable data fitting. The estimated magnetization direction also confirms the existence of remarkable remanent magnetization.

CONCLUSION

We have presented a new method for estimating the total magnetization direction of 3D magnetic sources from the total-field anomaly by using the equivalent-layer technique. Our method is formulated as an iterative least-squares problem and imposes a positivity constraint on the magnetic moments over the layer. Prior knowledge about the shape and depth of magnetic sources are not required, neither the use of an evenly spaced data. This methodology can be applied for determining the magnetization direction within multiple sources, considering all of them with the same magnetization direction. Moreover, we theoretically prove that a positive magnetic-moment distribution within an equivalent layer exists if it has the same magnetization direction of the true magnetic source, even if its purely induced or not.

By imposing the positivity constraint on the estimate of the magnetic-moment distribution over an equivalent-layer allows our method estimating the magnetization direction of magnetic sources. The results obtained with the synthetic data produced by unidirectional magnetized sources have shown the good performance of our method in retrieving the true magnetization direction. Tests simulating multiple sources and in the presence of shallow-seated source with a single or multiple magnetization directions produce good estimate of the total magnetization direction of magnetic sources, although they yield a large data misfit above the shallow source. Application to field data over the Goias alkaline province (GAP), center of Brazil, has confirmed that our method can be a reliable tool for interpreting real complex geological scenarios. The result over the alkaline complex giving rise to the Montes Claros de Goiás anomalies suggests the presence of a strong remanent magnetization component, in accordance to previous studies. Moreover, the all-positive

magnetic moment over the layer leads to very acceptable RTP anomalies. WWe consider that the locally large data-misfit in the real data application is due to shallow sources. Despite reliable magnetization direction estimate, we cannot infer if the shallow source has the same magnetization direction of other bodies.

APPENDIX A

CONSEQUENCES OF HIGH-LATITUDE ESTIMATION

One critical limitation for estimating the magnetization direction results of the case of estimating magnetization direction in high latitudes. In this appendix, we prove the existence of high latitude difficulties providing a theoretical basis and testing it on extreme cases.

The process of estimating magnetization direction using equivalent-layer technique is divided into two inversions. One by solving a constrained linear problem using positivity for magnetic-moment distribution and the other an unconstrained nonlinear estimation for magnetization direction. A way to extract infomations about the rank-deficiency and ill-conditioning of linear systems is exploring the singular value decomposition. This procedure allows an $N \times M$ matrix can be rewritten as the product of three matrices, one of them formed by the set of singular values arranged in order of decreasing size. The context of decomposing a matrix in singular values is to obtain pieces of information that can be estimated. It can also be useful to dictate which rows or columns of the matrix are linear independent. The fact is that, if a row or a column of a matrix is all null, it impacts directly on the linear dependence. Consequently, it leads to a rank-deficiency and an ill-conditioning of a linear system. Moreover, it is associated with zero singular values. Thus, the construction of the $N \times 2$ sensitivity matrix $\mathbf{G}_p^k$ is explicitly given by

$$\mathbf{G}_p^k = \begin{bmatrix} \mathbf{p}^{k^T} \partial_{\tilde{\imath}} \mathbf{g}_1(\mathbf{q}^k) & \mathbf{p}^{k^T} \partial_{\tilde{d}} \mathbf{g}_1(\mathbf{q}^k) \\ \vdots & \vdots \\ \mathbf{p}^{k^T} \partial_{\tilde{\imath}} \mathbf{g}_N(\mathbf{q}^k) & \mathbf{p}^{k^T} \partial_{\tilde{d}} \mathbf{g}_N(\mathbf{q}^k) \end{bmatrix}, \tag{A-1}$$

in which $\mathbf{p}^{k^T} \partial_\alpha \mathbf{g}_i(\mathbf{q}^k)$, $\alpha = \tilde{\imath}, \tilde{d}$, is a derivative in relation to inclination (first column)

and the declination (second column) evaluated at the ith observation point. That is, by calculating the derivative of equation 17 in relation to magnetization direction is in fact the derivative of the vector $\hat{\mathbf{m}}(\mathbf{q})$ (equation 5). The derivative of the vector $\hat{\mathbf{m}}(\mathbf{q})$ in relation to inclination is given by

$$\frac{\partial \hat{\mathbf{m}}(\mathbf{q})}{\partial \tilde{\mathrm{i}}} = \begin{bmatrix} -\sin\tilde{\mathrm{i}}\cos\tilde{d} \\ -\sin\tilde{\mathrm{i}}\sin\tilde{d} \\ \cos\tilde{\mathrm{i}} \end{bmatrix}, \tag{A-2}$$

and analogously for the declination is equal to

$$\frac{\partial \hat{\mathbf{m}}(\mathbf{q})}{\partial \tilde{d}} = \begin{bmatrix} -\cos\tilde{\mathrm{i}}\sin\tilde{d} \\ \cos\tilde{\mathrm{i}}\cos\tilde{d} \\ 0 \end{bmatrix}. \tag{A-3}$$

Hence, for the case whose the magnetization direction of the true magnetic source has inclination 90° and declination 0°, the equation A-2 and A-3 is, respectively, equal to

$$\frac{\partial \hat{\mathbf{m}}(\mathbf{q})}{\partial \tilde{\mathrm{i}}} = \begin{bmatrix} -1 \\ 0 \\ 0 \end{bmatrix}, \tag{A-4}$$

and

$$\frac{\partial \hat{\mathbf{m}}(\mathbf{q})}{\partial \tilde{d}} = \begin{bmatrix} 0 \\ 0 \\ 0 \end{bmatrix}. \tag{A-5}$$

We can notice from all these reasoning that the second row of the sensitivity matrix A-1 is all null for a vertical magnetization direction. Consequently, it leads to a rank-deficiency and the ill-conditioning of a linear system in this situation. However, its different for the extreme case of low latitude in which the magnetization direction has the inclination $0°$ and declination $0°$.

REFERENCES

Aster, R. C., B. Borchers, and C. H. Thurber, 2005, Parameter estimation and inverse problems (international geophysics): Academic Press.

Baratchart, L., D. P. Hardin, E. A. Lima, E. B. Saff, and B. P. Weiss, 2013, Characterizing kernels of operators related to thin-plate magnetizations via generalizations of Hodge decompositions: Inverse Problems, **29**, 015004(29pp).

Barnes, G., and J. Lumley, 2011, Processing gravity gradient data: GEOPHYSICS, **76**, I33–I47.

Bhattacharyya, B. K., 1966, A method for computing the total magnetization vector and the dimensions of a rectangular block shaped from magnetic anomalies: GEOPHYSICS, **31**, 74–96.

Blakely, R. J., 1996, Potential theory in gravity and magnetic applications: Cambridge University press.

Carlson, R. W., A. L. N. Araujo, T. C. Junqueira-Brod, J. C. Gaspar, J. A. Brod, I. A. Petrinovic, M. H. B. M. Hollanda, M. M. Pimentel, and S. Sichel, 2007, Chemical and isotopic relationships between peridotite xenoliths and maficultrapotassic rocks from southern brazil: Chemical Geology, **242**, 415 – 434.

Cordell, L., 1992, A scattered equivalent-source method for interpolation and gridding of potential-field data in three dimensions: GEOPHYSICS, **57**, 629–636.

Dampney, C. N. G., 1969, The equivalent source technique: GEOPHYSICS, **34**, 39–53.

Dannemiller, N., and Y. Li, 2006, A new method for determination of magnetization direction: GEOPHYSICS, **71**, L69–L73.

Dutra, A. C., Y. Marangoni, and R. I. F. Trindade, 2014, Aeromagnetic and physical-chemical properties of some complexes from GoiÃ¡s Alkaline Province: Brazilian Journal

of Geology, **44**, 361 – 373.

Emilia, D. A., and R. L. Massey, 1974, Magnetization estimation for nonuniformly magnetized seamounts: GEOPHYSICS, **39**, 223–231.

Fedi, M., G. Florio, and A. Rapolla, 1994, A method to estimate the total magnetization direction from a distortion analysis of magnetic anomalies1: Geophysical Prospecting, **42**, 261–274.

Gerovska, D., M. J. Arazo-Bravo, and P. Stavrev, 2009, Estimating the magnetization direction of sources from southeast bulgaria through correlation between reduced-to-the-pole and total magnitude anomalies: Geophysical Prospecting, **57**, 491–505.

Guspí, F., and I. Novara, 2009, Reduction to the pole and transformations of scattered magnetic data using newtonian equivalent sources: GEOPHYSICS, **74**, L67–L73.

H. Goldstein, C. P. P. J., and J. L. Safko, 1980, Classical mechanics: Addison-Wesley.

Hansen, P., and D. OLeary, 1993, The use of the l-curve in the regularization of discrete ill-posed problems: SIAM Journal on Scientific Computing, **14**, 1487–1503.

Hansen, R. O., and Y. Miyazaki, 1984, Continuation of potential fields between arbitrary surfaces: GEOPHYSICS, **49**, 787–795.

Junqueira-Brod, T. C., J. C. Gaspar, J. A. Brod, and C. V. Kafino, 2005, Kamafugitic diatremes: their textures and field relationships with examples from the gois alkaline province, brazil: Journal of South American Earth Sciences, **18**, 337 – 353. (Volcanic rocks in Brazil through time and different tectonic settings).

Lawson, C. L., and R. J. Hanson, 1974, Solving least squares problems: SIAM.

Leão, J. W. D., and J. B. C. Silva, 1989, Discrete linear transformations of potential field data: GEOPHYSICS, **54**, 497–507.

Lelivre, P. G., and D. W. Oldenburg, 2009, A 3d total magnetization inversion applicable

when significant, complicated remanence is present: GEOPHYSICS, **74**, L21–L30.

Li, S.-L., and Y. Li, 2014, Inversion of magnetic anomaly on rugged observation surface in the presence of strong remanent magnetization: GEOPHYSICS, **79**, J11–J19.

Li, Y., M. Nabighian, and D. W. Oldenburg, 2014a, Using an equivalent source with positivity for low-latitude reduction to the pole without striation: GEOPHYSICS, **79**, J81–J90.

———, 2014b, Using an equivalent source with positivity for low-latitude reduction to the pole without striation: GEOPHYSICS, **79**, J81–J90.

Li, Y., and D. W. Oldenburg, 2010, Rapid construction of equivalent sources using wavelets: GEOPHYSICS, **75**, L51–L59.

Lima, E. A., and B. P. Weiss, 2016, Ultra-high sensitivity moment magnetometry of geological samples using magnetic microscopy: Geochemistry, Geophysics, Geosystems, **17**, 3754–3774.

Lima, E. A., B. P. Weiss, L. Baratchart, D. P. Hardin, and E. B. Saff, 2013, Fast inversion of magnetic field maps of unidirectional planar geological magnetization: J. Geophys. Res.: Solid Earth, **118**, 2723–2752.

Liu, S., X. Hu, Y. Xi, T. Liu, and S. Xu, 2015, 2d sequential inversion of total magnitude and total magnetic anomaly data affected by remanent magnetization: GEOPHYSICS, **80**, K1–K12.

Marangoni, Y., H. Zhang, and H. Ferreira, 2016, Gravity and magnetic integrated data interpretation of the corrgo dos bois complex, gois alkaline province, central brazil: Revista Brasileira de Geofsica, **33**, 599–610.

Marangoni, Y. R., and M. S. Mantovani, 2013, Geophysical signatures of the alkaline intrusions bordering the paran basin: Journal of South American Earth Sciences, **41**, 83 – 98. (Alkaline Magmatism and the Lithospheric Mantle : a special issue in honour of the

work of Celso de Barros Gomes on the occasion of his 77th birthday).

Martinez, C., and Y. Li, 2016, Denoising of gravity gradient data using an equivalent source technique: GEOPHYSICS, **81**, G67–G79.

Medeiros, W. E., and J. B. C. Silva, 1995, Simultaneous estimation of total magnetization direction and 3-d spatial orientation: GEOPHYSICS, **60**, 1365–1377.

Mendonça, C. A., and J. B. C. Silva, 1994, The equivalent data concept applied to the interpolation of potential field data: GEOPHYSICS, **59**, 722–732.

Nabighian, M. N., V. J. S. Grauch, R. O. Hansen, T. R. LaFehr, Y. Li, J. W. Peirce, J. D. Phillips, and M. E. Ruder, 2005, The historical development of the magnetic method in exploration: GEOPHYSICS, **70**, 33ND–61ND.

Oliveira Jr., V. C., V. C. F. Barbosa, and L. Uieda, 2013, Polynomial equivalent layer: GEOPHYSICS, **78**, G1–G13.

Oliveira Jr, V. C., D. P. Sales, V. C. F. Barbosa, and L. Uieda, 2015, Estimation of the total magnetization direction of approximately spherical bodies: Nonlinear Processes in Geophysics, **22**, 215–232.

Parker, R. L., L. Shure, and J. A. Hildebrand, 1987, The application of inverse theory to seamount magnetism: Reviews of Geophysics, **25**, 17–40.

Pedersen, L. B., 1991, Relations between potential fields and some equivalent sources: GEOPHYSICS, **56**, 961–971.

Phillips, D. J., 2005, Can we estimate total magnetization directions from aeromagnetic data using helbig's integrals?: Earth, Planets and Space, **57**, 681–689.

Ryuji, K., and A. Uchiyama, 2005, Three-dimensional magnetization vector inversion of a seamount: Earth, Planets and Space, **57**, 691–699".

Silva, J. B. C., 1986, Reduction to the pole as an inverse problem and its application to

low-latitude anomalies: GEOPHYSICS, **51**, 369–382.

Siqueira, F. C. L., V. C. O. Jr., and V. C. F. Barbosa, 2017, Fast iterative equivalent-layer technique for gravity data processing: A method grounded on excess mass constraint: GEOPHYSICS, **82**, G57–G69.

Tontini, F. C., and L. B. Pedersen, 2008, Interpreting magnetic data by integral moments: Geophysical Journal International, **174**, 815–824.

Weiss, B. P., E. A. Lima, L. E. Fong, and F. J. Baudenbacher, 2007, Paleomagnetic analysis using squid microscopy: Journal of Geophysical Research: Solid Earth, **112**, n/a–n/a. (B09105).

Zhang, H., D. Ravat, Y. R. Marangoni, G. Chen, and X. Hu, 2018, Improved total magnetization direction determination by correlation of the normalized source strength derivative and the rtp fields: GEOPHYSICS, **0**, 1–45.

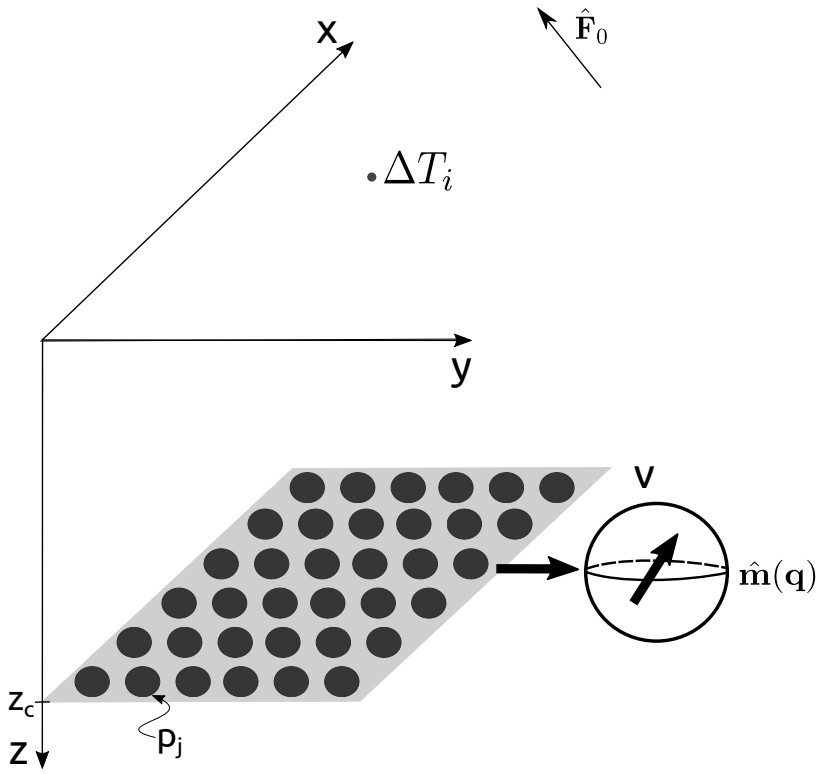

Figure 1: Schematic representation of an equivalent layer. The layer is positioned over the horizontal plane at a depth of $z = z_c$. $\Delta T_i = f_i(\mathbf{s})$ is the predicted total-field anomaly at the point (x_i, y_i, z_i) produced by the set of M equivalent sources (black dots). Each source is located at the point (x_j, y_j, z_c), $j = 1, \ldots, M$, and represented by a dipole with unity volume υ with magnetization direction $\hat{\mathbf{m}}(\mathbf{q})$ and magnetic moment p_j.

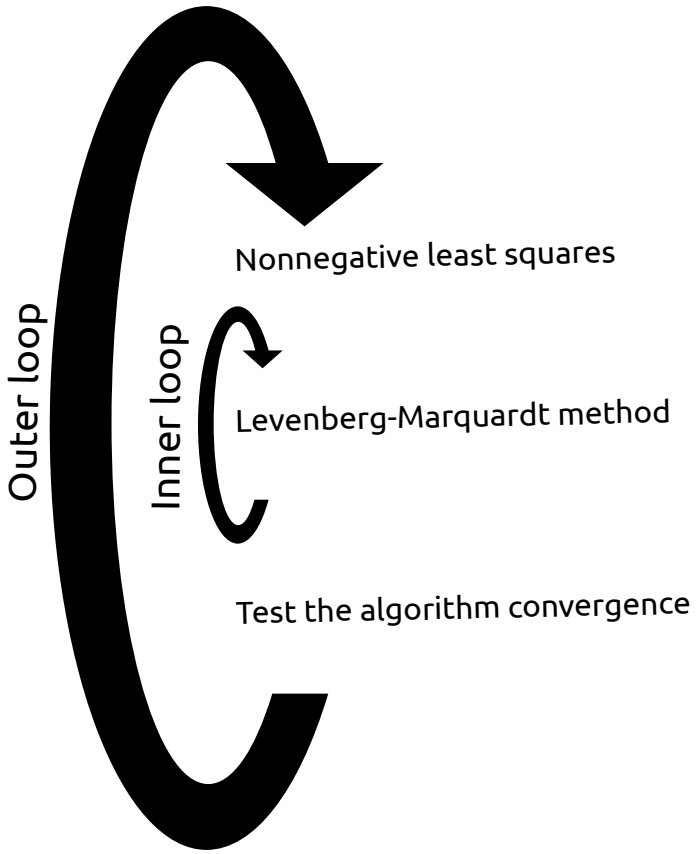

Figure 2: Iterative scheme overview for NNLS and Levenberg-Marquardt method for estimating magnetization direction. The outer loop is the nonnegative solution for magnetic-moment distribution and the inner loop calculates the magnetization direction correction using Levenberg-Marquardt method.

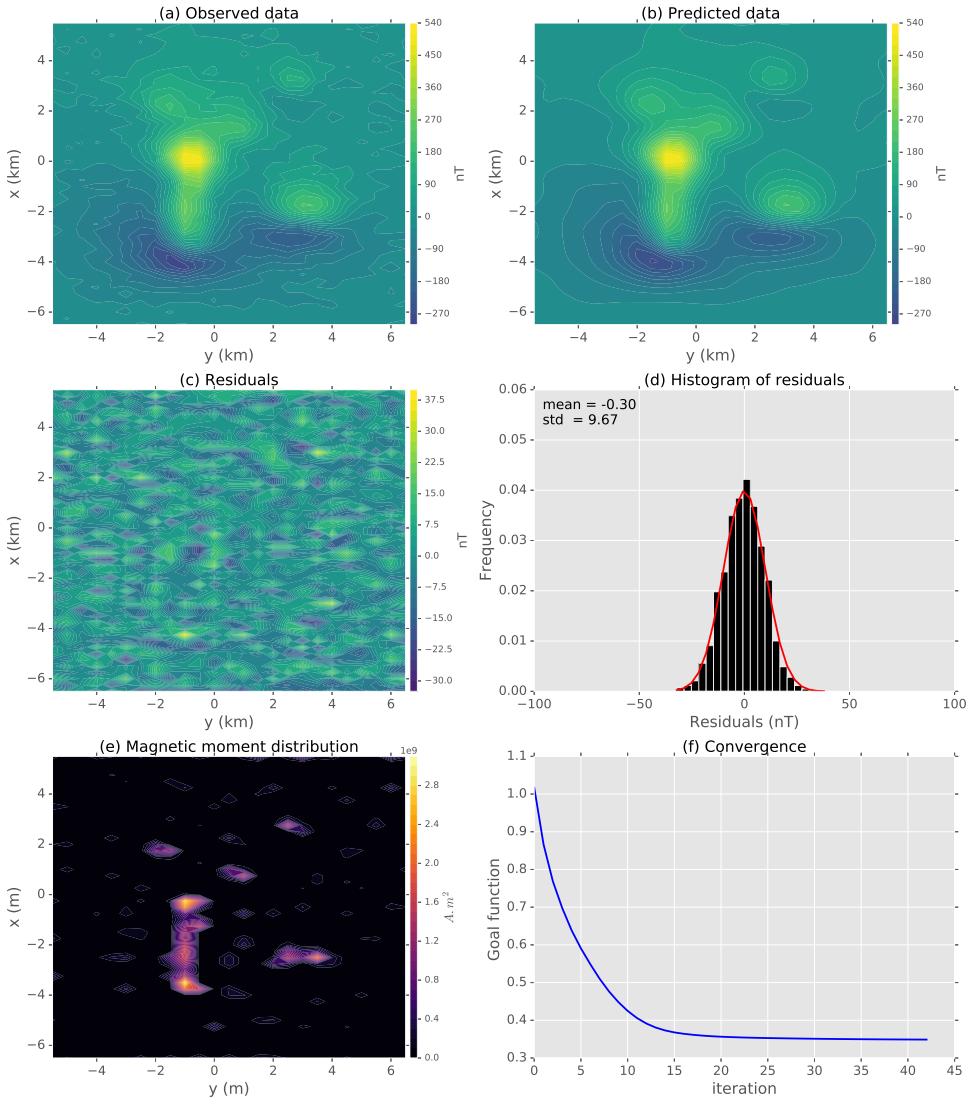

Figure 3: Application to synthetic data for multiple sources with unidirectional magnetization. (a) Noise-corrupted total-field anomaly. (b) Predicted data produced by equivalent layer. (c) Difference between the data shown in panels a and b. (d) Histogram of residuals. (e) All-positive magnetic-moment distribution. (f) Goal function value (equation 19a) per iteration showing the convergence.

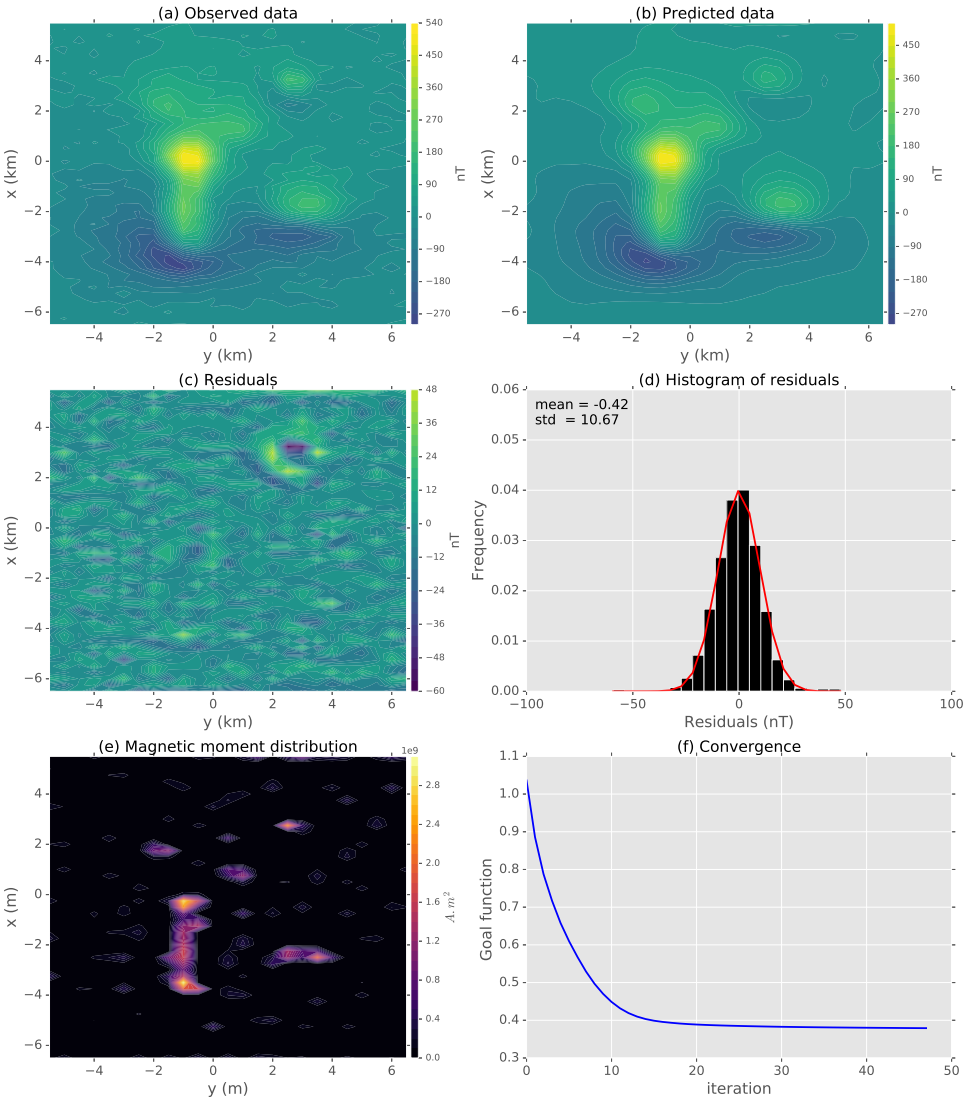

Figure 4: Multiple synthetic sources with a shallow-seated body under unidirectional magnetization . (a) Noise-corrupted total-field anomaly. (b) Predicted data produced by equivalent layer. (c) Difference between the data shown in panels a and b. (d) Histogram of residuals. (e) All-positive magnetic-moment distribution. (f) Goal function value (equation 19a) per iteration showing the convergence.

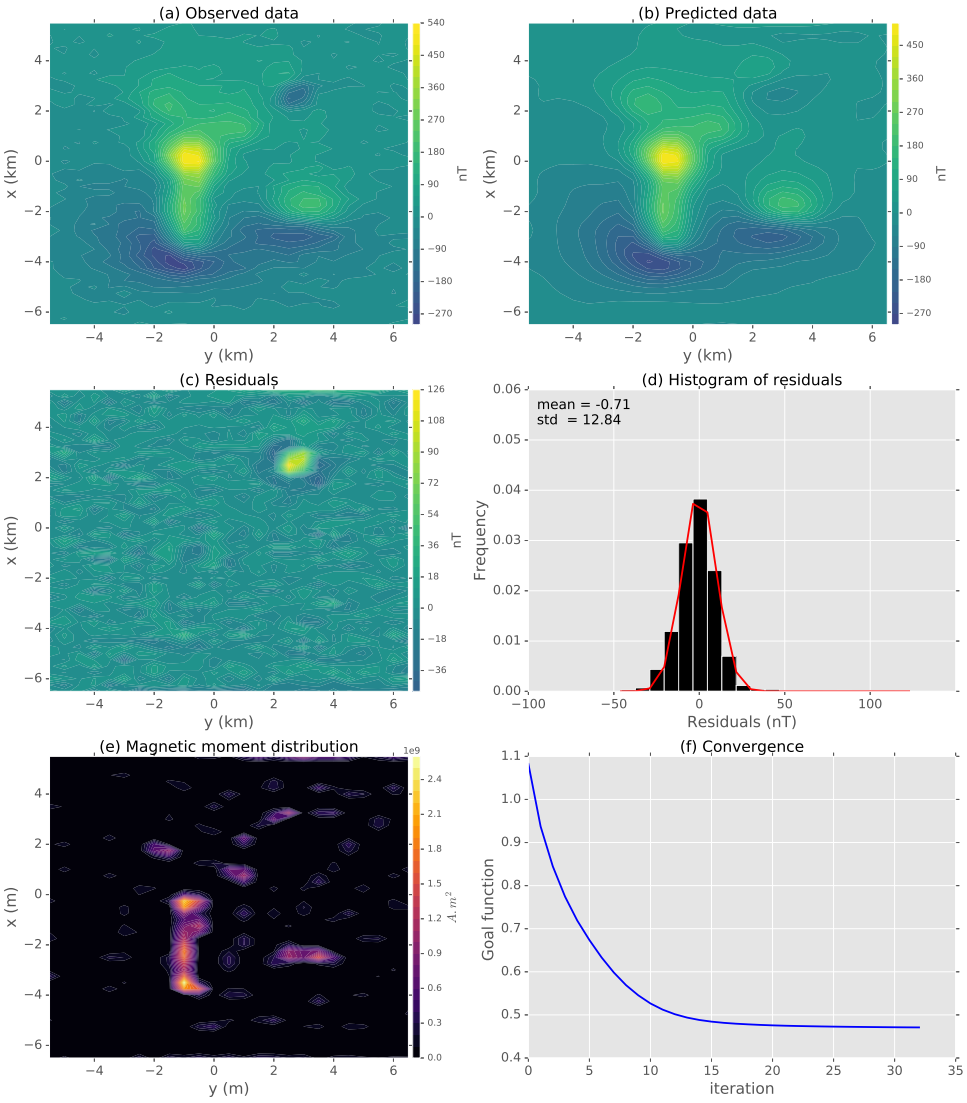

Figure 5: Multiple synthetic sources with a shallow-seated body under different magnetization directions. (a) Noise-corrupted total-field anomaly. (b) Predicted data produced by equivalent layer. (c) Difference between the data shown in panels a and b. (d) Histogram of residuals. (e) All-positive magnetic-moment distribution. (f) Goal function value (equation 19a) per iteration showing the convergence.

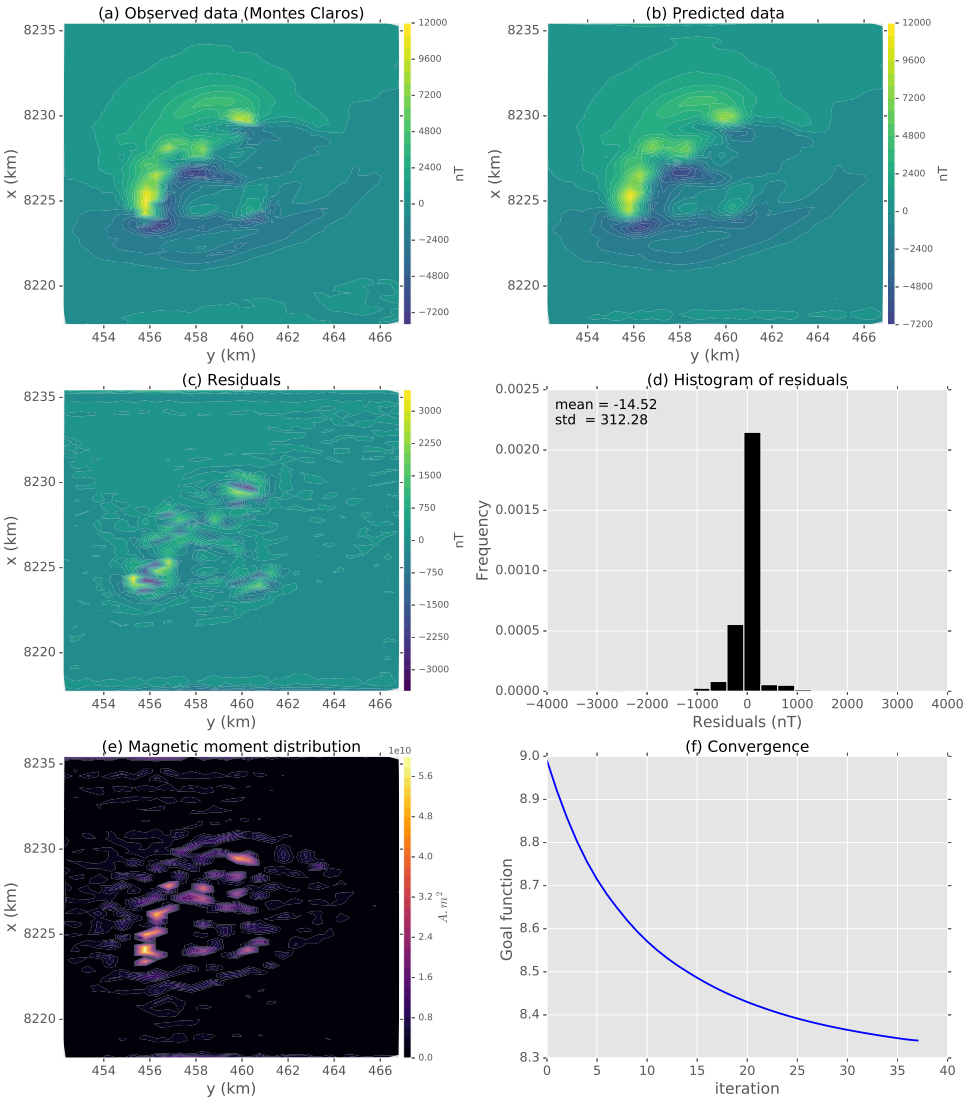

Figure 6: Application to field data from alkaline complex of Montes Claros (Brazil). (a) Observed total-field anomaly. (b) Predicted data produced by equivalent layer. (c) Difference between the data shown in panels a and b. (d) Histogram of residuals. (e) All-positive magnetic-moment distribution. (f) Goal function value (equation 19a) per iteration showing the convergence.

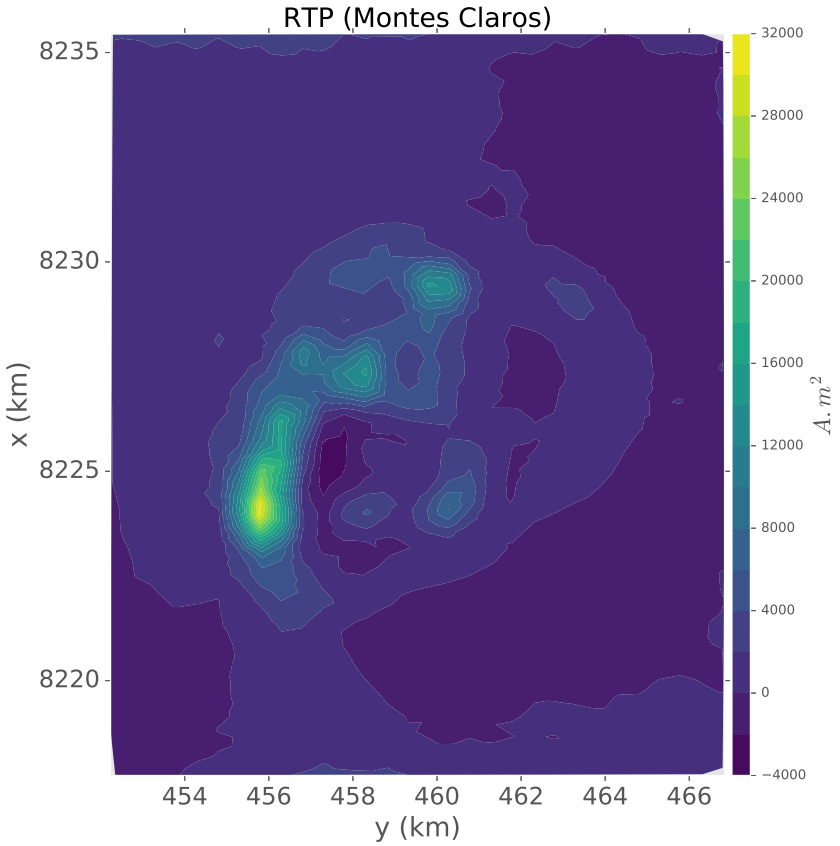

Figure 7: Application to field data from alkaline complex of Montes Claros (Brazil). RTP anomaly computed by using the estimated magnetization distribution shown in figure 6e.